RESEARCH ARTICLE

Acquired and intrinsic resistance to vemurafenib in BRAF^{V600E}-driven melanoma brain metastases

Ping Zhang[1,2,3], Laura Esmee Kuil[1,4] (iD), Levi Conrad Maria Buil[1,5], Stephan Freriks[1,5], Jos Hendrik Beijnen[6,7] (iD), Olaf van Tellingen[1,5] (iD) and Mark Cornelis de Gooijer[1,8,9] (iD)

1 Division of Pharmacology, The Netherlands Cancer Institute, Amsterdam, The Netherlands
2 Department of Neurosurgery, Qilu Hospital, Cheeloo College of Medicine and Institute of Brain and Brain-Inspired Science, Shandong University, China
3 Shandong Provincial Key Laboratory of Brain Function Remodeling, Qilu Hospital, Shandong University, China
4 Division of Psychosocial Sciences and Epidemiology, The Netherlands Cancer Institute, Amsterdam, The Netherlands
5 Mouse Cancer Clinic, The Netherlands Cancer Institute, Amsterdam, The Netherlands
6 Department of Pharmacy and Pharmacology, The Netherlands Cancer Institute/MC Slotervaart Hospital, Amsterdam, The Netherlands
7 Division of Pharmacoepidemiology and Clinical Pharmacology, Department of Pharmaceutical Sciences, Faculty of Science, Utrecht University, The Netherlands
8 Faculty of Biology, Medicine and Health, University of Manchester, UK
9 The Christie NHS Foundation Trust, Manchester, UK

$BRAF^{V600}$-mutated melanoma brain metastases (MBMs) are responsive to BRAF inhibitors, but responses are generally less durable than those of extracranial metastases. We tested the hypothesis that the drug efflux transporters P-glycoprotein (P-gp; ABCB1) and breast cancer resistance protein (BCRP; ABCG2) expressed at the blood–brain barrier (BBB) offer MBMs protection from therapy. We intracranially implanted A375 melanoma cells in wild-type (WT) and $Abcb1a/b;Abcg2^{-/-}$ mice, characterized the tumor BBB, analyzed drug levels in plasma and brain lesions after oral vemurafenib administration, and determined the efficacy against brain metastases and subcutaneous lesions. Although contrast-enhanced MRI demonstrated that the integrity of the BBB is disrupted in A375 MBMs, vemurafenib achieved greater antitumor efficacy against MBMs in $Abcb1a/b;Abcg2^{-/-}$ mice compared with WT mice. Concordantly, P-gp and BCRP are expressed in MBM-associated brain endothelium both in patients and in A375 xenografts and expression of these transporters limited vemurafenib penetration into A375 MBMs. Although initially responsive, A375 MBMs rapidly developed therapy resistance, even in $Abcb1a/b;Abcg2^{-/-}$ mice, and this was unrelated to pharmacokinetic or target inhibition issues. Taken together, we demonstrate that both intrinsic and acquired resistance can play a role in MBMs.

Metastatic melanoma patients historically have a poor survival, mostly due to a lack of available effective chemotherapeutics [1]. However, in the last decade significant advances have been made that considerably improved the outlook for metastatic melanoma patients. These advances were kick-started by the discovery of oncogenic *BRAF* mutations as an important driver in melanoma [2]. The vast majority of *BRAF* mutations are

Abbreviations

AUC, area under the curve; BBB, blood–brain barrier; BCRP, breast cancer resistance protein; CSF, cerebrospinal fluid; MBM, melanoma brain metastasis; MEM, minimum essential medium; MRI, magnetic resonance imaging; P-gp, P-glycoprotein; WT, wild-type.

in codon 600, substituting a valine for either a glutamic acid, lysine, arginine, or aspartic acid, and result in constitutively active $BRAF^{V600E/K/R/D}$ oncoproteins [3]. $BRAF^{V600}$-positive melanoma cells can therefore proliferate independently from external growth stimuli [2]. Importantly, $BRAF^{V600}$ can be therapeutically targeted, and three drugs have now been approved for treatment of metastatic melanoma: vemurafenib [4], dabrafenib [5], and encorafenib [6]. All three $BRAF^{V600}$ inhibitors have generated striking clinical responses and significantly improved survival of metastatic melanoma patients [7–9]. However, therapy resistance invariably occurs, in most cases due to selection and outgrowth of clones that carry additional mutations more downstream in the MAPK signaling pathway [10]. Therefore, BRAF inhibitors are currently successfully combined with MEK inhibitors (vemurafenib and cobimetinib [11], dabrafenib and trametinib [12], and encorafenib and binimetinib [6]), yielding further improved response rates and survival [13–15].

Despite all the recent success in treatment of metastatic melanoma, it is still unclear whether patients with melanoma brain metastases (MBMs) benefit similarly from $BRAF^{V600}$ inhibitors as metastatic melanoma patients with extracranial metastases. In the clinical studies that led to the approval of $BRAF^{V600}$ inhibitors for metastatic melanoma, MBM patients were excluded from study participation. Only recently, clinical trials focusing specifically on MBM patients have been set up, and the results from several phase II trials appear to suggest that $BRAF^{V600}$ inhibitors also induce responses in MBMs [16,17]. However, these responses were generally shorter than those achieved in extracranial metastases, suggesting that resistance occurs in MBMs even more rapidly than in extracranial metastases [17]. The reason for this rapid resistance in MBMs is unclear, but could be related to the brain environment. Several preclinical studies have demonstrated that vemurafenib [18,19], dabrafenib [20], and encorafenib [21] exhibit very poor brain penetration in mice as a result of efficient efflux by P-glycoprotein (P-gp; ABCB1) and breast cancer resistance protein (BCRP; ABCG2) at the blood–brain barrier (BBB). These observations seem to be corroborated by a clinical study showing that the concentration of vemurafenib in cerebrospinal fluid (CSF) was < 1% of the plasma concentration [22].

The BBB limits the brain penetration of many xenobiotics, including many anticancer agents [23], and can consequently impact the intracranial anticancer efficacy of small molecule drugs [24,25]. Importantly, drug efflux transporters can restrict drug delivery and efficacy even when the BBB is considered 'leaky' [26].

We therefore here investigate the impact of P-gp and BCRP on the efficacy of vemurafenib against MBMs in an intracranial mouse model of $BRAF^{V600E}$-driven melanoma. In line with the clinical data, we find that MBMs can respond to vemurafenib, most likely as a result of compromised BBB integrity. However, vemurafenib achieved greater antitumor responses in $Abcb1a/b;Abcg2^{-/-}$ mice, indicating that P-gp and BCRP still play a protective role at the compromised BBB of MBMs. Supporting this hypothesis, we find that P-gp and BCRP are expressed in MBM-associated brain endothelium both in patients and intracranial xenografts in mice. Importantly, vemurafenib efficacy could be improved by co-administration of the P-gp/BCRP inhibitor elacridar, offering a potential clinical strategy for increasing vemurafenib efficacy against MBMs. Intriguingly, we also observed much more rapid therapy resistance in the preclinical MBM model compared with previously published extracranial melanoma mouse models, analogous to clinical observations. We conclude that $BRAF^{V600}$-positive MBMs are not only less responsive to vemurafenib because drug efflux transporters at the BBB limit drug penetration into the tumor, but also because they can rapidly acquire resistance during treatment. Therefore, P-gp/BCRP inhibitors might help to improve the clinical response of MBMs to vemurafenib by increasing its brain penetration, but pinpointing the mechanism behind the brain-specific acquired resistance will likely be necessary to produce durable responses.

Methods

Cell culture and drugs

A375 (RRID: CVCL_0132), K1735 (RRID: CVCL_F828), and Mel57 (RRID: CVCL_4454) cells expressing firefly luciferase and mCherry were cultured in minimum essential medium (MEM) supplemented with 10% fetal bovine serum (FBS), 1% penicillin/streptomycin, L-glutamine, non-essential amino acids, sodium pyruvate, and MEM vitamins (all Life Technologies, Carlsbad, CA, USA). Mel57 cells were kindly provided by W. P. Leenders (Radboud University Medical Center, Nijmegen, the Netherlands), and K1735 and A375 were a gift from I. J. Fidler (MD Anderson Cancer Center, Houston, TX, USA). A375 and Mel57 cell lines have been authenticated by STR profiling using the GenePrint 10 system (Promega, Madison, WI, USA) and were cultured mycoplasma-free, as confirmed by PCR. All cell lines were also tested negative for mouse pathogens by Impact I PCR profile (2) (IDEXX, Ludwigsburg, Germany). Vemurafenib was purchased from LC Laboratories (Woburn, MA, USA), vemurafenib-$^{13}C6$ was obtained from the Slotervaart Hospital pharmacy, and

elacridar was generously provided by GlaxoSmithKline (Research Triangle Park, NC, USA).

Animals

Mice were housed and handled according to institutional guidelines complying with Dutch and European legislation. All experiments with animals were approved by the Animal Welfare Body of the Netherlands Cancer Institute under DEC protocol 12.019. The animals were either athymic (nude) mice of a > 99% FVB background with wild-type (WT) or *Abcb1a/b;Abcg2$^{-/-}$* genotype or C3H/HeN, between 8 and 12 weeks of age. The animals were kept in a temperature-controlled environment at 20.9 °C on a 12 h light/dark cycle and received chow and acidified water *ad libitum*.

Drug formulations

A stock solution (25 or 10 mg·mL^{-1}) of vemurafenib was dissolved in dimethyl sulfoxide (DMSO) and Cremophor EL (1 : 1; both Sigma-Aldrich, St. Louis, MO, USA). The working solution (2.5 or 1 mg·mL^{-1}) was freshly prepared prior to administration by diluting the stock solution with saline on the day of administration. Elacridar (5 mg·mL^{-1}) was formulated in DMSO : Cremophor EL : water (1 : 2 : 7) and prepared similarly.

Xenograft models and tumor growth monitoring

For subcutaneous xenograft models, 30 μL of cell suspension containing 3×10^6 A375 cells was injected into both flanks of FVB WT and *Abcb1a/b;Abcg2$^{-/-}$* nude mice. For xenograft MBM models, stereotactic intracranial injections (A375 and Mel57) or intracarotid injections (K1735) of melanoma cells were performed as described previously [24,27]. For intracranial injections, FVB nude mice were injected intracranially with 2 μL of A375 or Mel57 cell suspension containing 1×10^5 cells 2 mm lateral, 1 mm anterior, and 3 mm ventral from the bregma. For intracarotid injections, 1×10^5 cells in 100 μL HBSS were injected in the left common carotid artery of C3H/HeN mice. Tumor growth was measured by bioluminescence imaging (BLI) for intracranial tumors and by caliper for subcutaneous tumors. The volume of subcutaneous tumors was calculated in mm^3 using the modified ellipsoid formula (volume = 0.5 × length × width^2). Bioluminescence images were acquired following i.p. D-luciferin (150 mg·kg^{-1}; Promega) using an IVIS 200 or IVIS Spectrum system with LIVING IMAGE software v4.5 (both PerkinElmer, Waltham, MA, USA). Animals were stratified into treatment groups to achieve a similar mean bioluminescence reading within each cohort. The bioluminescence intensity of each individual animal on the day of the start of treatment (Day 0) was arbitrarily set at 100%. All subsequent measurements were recorded relative to this first

measurement and converted to their log values. Mean ± standard error (SE) values were calculated and plotted in graphs.

Magnetic resonance imaging

A BioSpec 70/20 USR (Bruker, Billerica, MA, USA) system was used for magnetic resonance imaging (MRI), as described previously [24]. The MRI sequence consisted of T2-weighted, T1-weighted precontrast, and T1-weighted postcontrast imaging. Gadoterate meglumine (Dotarem®; Guerbet, Villepinte, France) diluted fivefold with saline was used as a contrasting agent and delivered via an intravenous cannula inserted in the tail vein. Mice were anesthetized using isoflurane (Pharmachemie B.V., Haarlem, the Netherlands) delivered via a customized mouse holder, and heart rate and breathing frequency were monitored throughout the entire procedure. PARAVISION software (v 6.0.1; Bruker) was used for image acquisition and FIJI [28] (v 1.49b) was used for image processing.

Pharmacokinetic studies

To establish vemurafenib plasma kinetics, tumor-free FVB WT, and *Abcb1a/b;Abcg2$^{-/-}$* nude mice received vemurafenib orally (p.o.) by gavage at indicated doses. Elacridar (100 mg·kg^{-1}) was administered p.o. by gavage 4 h before vemurafenib. Blood was sampled from the tail vein at 15 min, 1, 2, 4, 8, and 24 h after the administration. The plasma was obtained by centrifugation (5 min, 2000 *g*, 4 °C). Vemurafenib was extracted from plasma by diethyl ether liquid–liquid extraction. Extracts were dried using a Savant SpeedVac Concentrator (Thermo Fisher Scientific, Waltham, MA, USA), reconstituted in MeCN : water (30 : 70), and subjected to liquid chromatography/tandem mass spectrometry (LC/MS–MS) analysis. Vemurafenib-^{13}C6 was used as an internal standard.

To study its distribution in tumor-bearing mice, vemurafenib was administered p.o. to tumor-bearing mice for 3 days at a dose of 10 or 25 mg·kg^{-1} q.d., starting 14 days after intracranial tumor cell injection. One group of mice received 10 mg·kg^{-1} vemurafenib 4 h after administration of 100 mg·kg^{-1} elacridar. Four hours after the third administration, blood was collected by heart puncture, and whole brains were dissected and divided into four parts: ipsilateral hemisphere (tissue from the tumor-bearing hemisphere that was free of macroscopic tumor tissue), contralateral hemisphere (the tumor-free hemisphere), cerebellum and macroscopic tumor. In a follow-up experiment, tissues and plasma were collected 4 h after 5 and 10 consecutive daily p.o. administrations of vemurafenib. All tissues were weighed and subsequently homogenized using a FastPrep®-24 (MP-Biomedicals, Irvine, CA, USA) in 3 mL 1% (w/v) bovine serum albumin. All tissue samples were prepared for LC–MS/MS analysis as described above for plasma samples.

LC–MS/MS analysis

The LC–MS/MS system consisted of an API 3000 mass spectrometer (Sciex, Framingham, MA, USA) coupled to an UltiMate 3000 LC System (Dionex, Sunnyvale, CA, USA). Samples were separated using a ZORBAX Extend-C18 column (Agilent, Santa Clara, CA, USA), preceded by a Securityguard C18 precolumn (Phenomenex, Utrecht, the Netherlands). Elution was done using a mixture of mobile phase A (0.1% formic acid in water (v/v)) and mobile phase B (methanol) in a 5 min gradient from 20% to 95% B, followed by 95% B that was maintained for 3 min and then re-equilibrated at 20% B. Multiple reaction monitoring parameters were 490.2/383.1 (vemurafenib) and 496.2/389.1 (vemurafenib-$^{13}C_6$). System control and data analysis were done using ANALYST® 1.6.2 software (AB Sciex, Foster City, CA, USA).

Efficacy studies in xenograft models

For the subcutaneous tumor model, therapy was initiated 2 weeks after implantation, when the tumor volume exceeded 40 mm^3. FVB WT and *Abcb1a/b;Abcg2$^{-/-}$* nude mice ($n = 8$) received 25 and 10 mg·kg^{-1} of vemurafenib daily, respectively. Control mice ($n = 8$) received vehicle. Tumor development was assessed by caliper twice a week. For the intracranial tumor model, treatment was started about 2 weeks after intracranial injection of tumor cells, when full-blown tumors were present in all animals. WT and *Abcb1a/b;Abcg2$^{-/-}$* nude mice received vehicle, 25 mg·kg^{-1} vemurafenib, 10 mg·kg^{-1} vemurafenib plus 100 mg·kg^{-1} ela-cridar, or 10 mg·kg^{-1} vemurafenib once daily for 10 consecutive days or in a 5 days on/2 days off/5 days on schedule, as indicated in the relevant figure panels. Tumor growth was monitored by BLI every 4 or 5 days. Mice were weighed daily weighed examined for abnormalities. The mice were humanely sacrificed based on BLI results or when weight loss exceeded 20% of the initial body weight.

Histology, immunohistochemistry, and image quantification

Mouse brains were fixed in 4% (v/v) formaldehyde. Alternatively, whole heads without skin were fixed in 4% (v/v) formaldehyde and 5% (v/v) glacial acetic acid and subsequently decalcified using a 6.5% (v/v) formic acid solution for 3 days at 37 °C. After fixation, samples were paraffin embedded and sliced into 4 μm thick sections. Whole head slides were stained for hematoxylin and eosin (H&E), human vimentin (1 : 4000; M0725; Dako-Cytomation, Glostrup, Denmark), P-gp (1 : 200; 13978; Cell Signaling Technology, Danvers, MA, USA), BCRP (1 : 400; ab24115; Abcam, Cambridge, UK), and CD31 (1 : 200; ab28364; Abcam). Vessel positivity for P-gp, BCRP, and CD31, as quantified in Fig. 1B, was manually scored in at least 200 vessels per staining. Specific antibody staining for P-gp and BCRP was validated previously using whole head slices from *Abcb1a/b;Abcg2$^{-/-}$* mice (fig. S2 from [26]).

Brain slides were stained for H&E, PDGFRβ (1 : 50; 3169; Cell Signaling Technology), phospho-MET (1 : 150; 3077; Cell Signaling Technology), MET (1 : 100; AF527; R&D Systems, Minneapolis, MN, USA), phospho-IGF1R (1 : 40 000; sc-101703; Santa Cruz Biotechnology, Dallas, TX, USA), AXL (1 : 100; 8661; Cell Signaling Technology), NGFR (1 : 400; 8238; Cell Signaling Technology), phospho-EGFR (1 : 600; ab40815; Abcam), EGFR (1 : 200; ab52894; Abcam), BRAF^{V600E} (1 : 100; E19290; SpringBioscience, Pleasanton, CA, USA), phospho-ERK1/2 (1 : 200; 4370; Cell Signaling Technology), phospho-AKT (1 : 8000; 4060; Cell Signaling Technology), phospho-S6 (1 : 1000; 2211; Cell Signaling Technology), phospho-4EBP1 (1 : 100; 2855; Cell Signaling Technology), 4EBP1 (1 : 1200; 9644; Cell Signaling Technology), SOX10 (1 : 100; sc-17342; Santa Cruz Biotechnology), MITF (1 : 100; 284 M-94; Cell Marque, Rocklin, CA, USA), and Ki-67 (1 : 3000; ab15580; Abcam).

Fig. 1. Characterization of the A375 melanoma brain metastasis model. (A) T2-weighted, T1-weighted precontrast, and T1-weighted post-gadolinium (Gd) contrast magnetic resonance imaging of A375 tumors grafted in the brains of wild-type (WT) nude mice. The tumor is indicated by the white arrow. (B) Histochemical staining with hematoxylin and eosin (H&E) and immunohistochemical staining of human vimentin (hVimentin), P-glycoprotein (P-gp), breast cancer resistance protein (BCRP), and CD31 of intracranial A375 melanoma tumors. Pie charts represent quantifications of positively and negatively stained vessels within A375 tumors. Scale bars represent 100 μm (top panels) and 20 μm (bottom panels). Sample sizes are indicated in the relevant panels. (C) Histochemical staining with hematoxylin and eosin (H&E) and immunohistochemical staining of human vimentin (hVimentin), P-gp, BCRP, and CD31 of intracranial K1735 and Mel57 melanoma tumors. Scale bars represent 100 μm (top panels) and 20 μm (bottom panels). (D) Analysis of *ABCB1*, *ABCG2*, and *CD31* gene expression by endothelial cells in brain and skin lesions from metastatic melanoma patients. Single-cell RNA-Seq data was reported by Smalley *et al.* [29] Sample sizes are indicated in the relevant panels. Differences in fractions of *ABCB1*, *ABCG2*, and *CD31* expressing cells between brain and skin lesions were compared using the Binomial test in which the skin fraction was considered as expected and the brain fraction was considered as observed. Correlations between *ABCB1* and *ABCG2* expression were determined using simple linear regression.

(A)

(B)

(C)

(D)
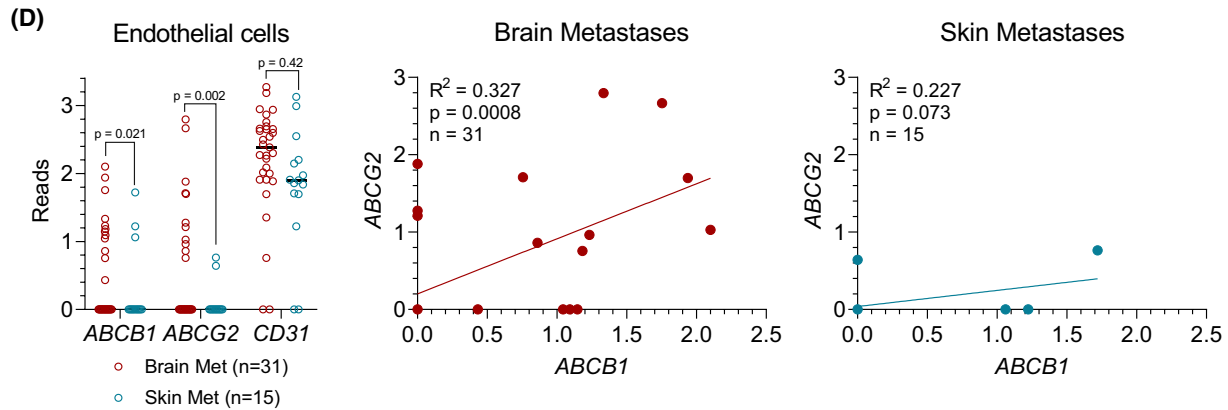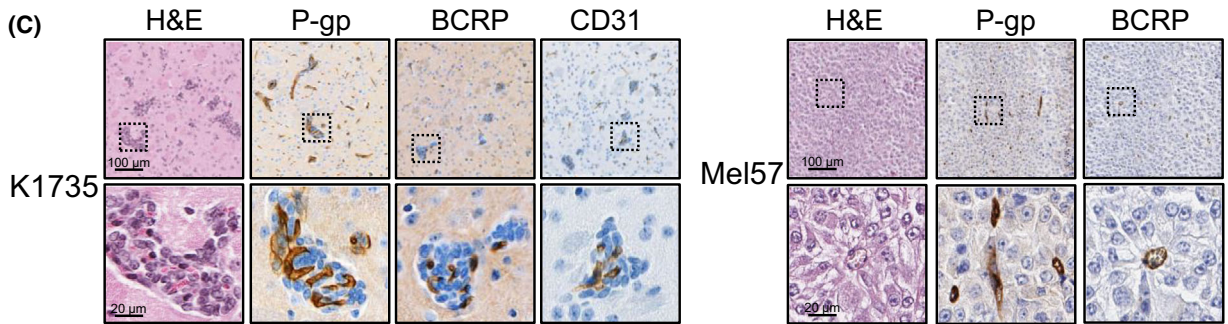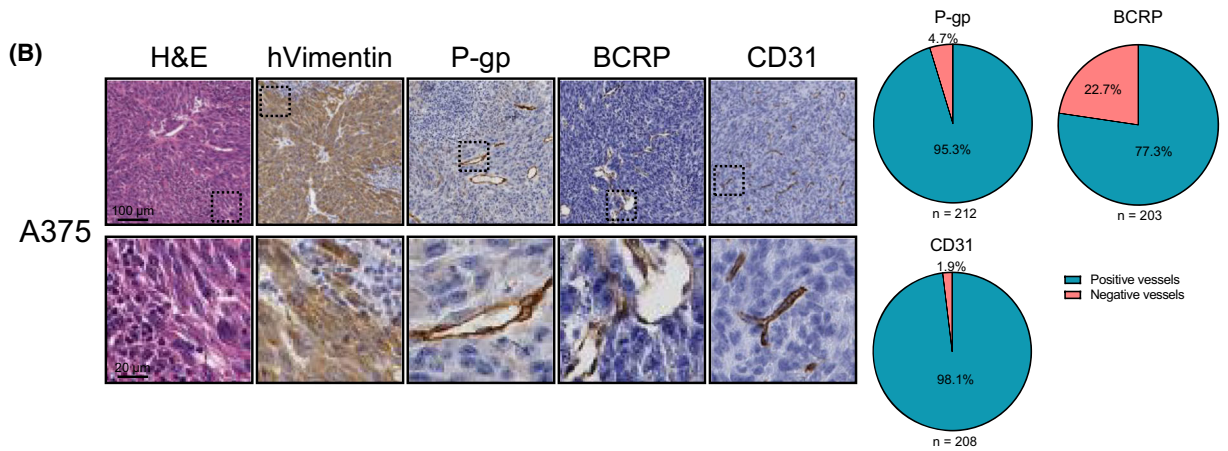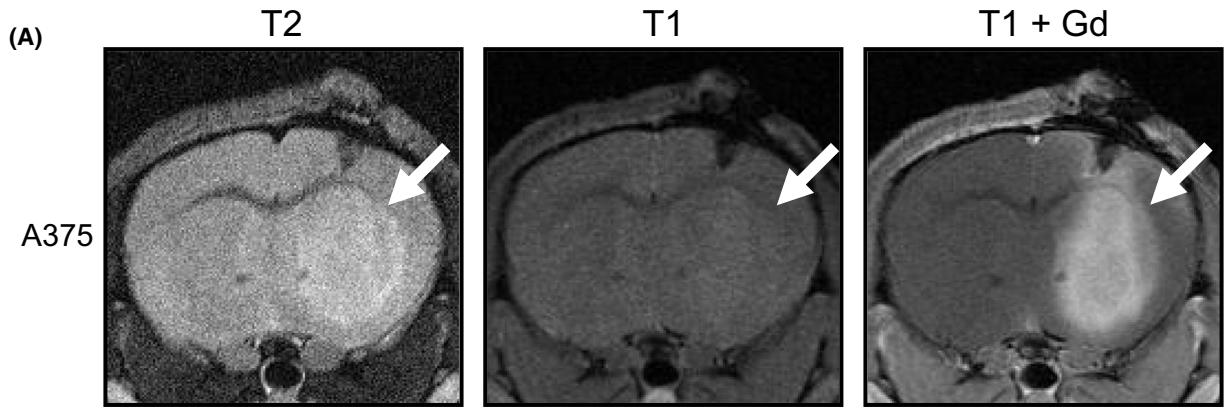
Single-cell RNA-Seq data analysis

Single-cell RNA-Seq data from brain and skin lesions from metastatic melanoma patients as reported by Smalley *et al.* were accessed from http://iscva.moffitt.org [29].

Pharmacokinetic calculations and statistical analysis

Pharmacokinetic parameters were calculated with PKSOLVER [30]. All comparisons involving more than two groups were analyzed by one-way ANOVA followed by Bonferroni *post hoc* tests. Differences in fractions of ABC transporter-expressing cells between brain and skin lesions were compared using the Binomial test in which the skin fraction was considered as expected and the brain fraction was considered as observed. Correlations were determined using simple linear regression. Kaplan–Meier curves were drawn using GRAPHPAD PRISM v7 (GraphPad Software, La Jolla, CA, USA), and statistically significant survival differences were determined using the log-rank test. Statistical significance was accepted in all tests when $P < 0.05$.

Results

Characterization of the A375 melanoma brain metastasis model

To characterize the BBB integrity of the A375 MBM model, we subjected mice that were intracranially injected with A375-FM cells to magnetic resonance imaging and (immuno)histochemical analysis. Similar to the clinical presentation of MBMs, intracranial A375 tumors were visible on T2-weighted and T1-weighted postgadolinium contrast MRI sequences (Fig. 1A). Enhancement on T1-weighted MR images after intravenous administration of a contrast agent indicates a reduction in BBB integrity. However, the BBB is not only a physical barrier but also a physiological barrier because of the expression of a range of efflux transporters, of which P-gp and BCRP are the most dominant. Immunohistochemical staining of these transporters in intracranial A375 tumors revealed that the majority of the vasculature in these tumors expresses P-gp and BCRP, as well as the endothelial cell marker CD31, suggesting that the physiological component of its BBB may still be functional (Fig. 1B). Expression of P-gp and BCRP in the vasculature of MBMs was confirmed in K1735 and Mel57 tumors, two other independent MBM models, and in line with our previous observations (Fig. 1C) [26]. Interestingly, intracranial A375 tumors were also characterized by large infiltrations of cells that resembled neutrophils, as apparent from their morphology and lack of staining for human vimentin. Melanomas are generally considered to be highly immunogenic, and widespread neutrophil infiltration could be a result of the immunogenicity of the A375 model.

To assess whether the A375 MBM model faithfully resembles ABC transporter expression at the BBB of MBMs in patients, we analyzed single-cell RNA-Seq data from melanoma brain and skin metastases recently reported by Smalley *et al.* [29]. Although these datasets, unfortunately, do not contain large numbers of endothelial cells, they suggest that P-gp/ABCB1 and BCRP/ABCG2 are expressed in MBM-associated endothelial cells, albeit heterogeneously (Fig. 1D). Importantly, hardly any expression was found in endothelial cells from skin metastases, suggesting that these transporters do not have an impact on skin lesions. Finally, we could also observe that endothelial cells associated with brain metastases tended to co-express P-gp and BCRP to similar extents, while this correlation did not occur in the relatively few endothelial cells from skin metastases that express P-gp or BCRP. Together, the observations from the Smalley *et al.* dataset led us to conclude that the A375 MBM model recapitulates the P-gp and BCRP expression found in MBM patients.

Vemurafenib has intrinsic antitumor potential against intracranial A375 tumors

The brain penetration of vemurafenib was previously reported to be significantly higher (between approximately 20- and 80-fold) in $Abcb1a/b;Abcg2^{-/-}$ compared with WT mice [18,19]. We therefore first studied the efficacy of vemurafenib treatment against A375 tumors implanted in the brains of $Abcb1a/b;Abcg2^{-/-}$ mice, as we expected these mice to be the most pharmacologically favorable recipients to establish the intrinsic antitumor potential of vemurafenib against MBMs. Indeed, two cycles of 5 days of 25 mg·kg^{-1} daily oral vemurafenib induced regression and subsequent tumor stasis of A375 tumors in these mice (Fig. 2A), without affecting body weight (Fig. S1A). When the treatment was stopped, tumor growth started at a similar speed as untreated tumors, but a survival difference was already established (Fig. 2B), indicating that vemurafenib is intrinsically potent against MBMs.

Dose adaptions between WT and *Abcb1a/b; Abcg2*$^{-/-}$ mice are needed to level the systemic exposure of vemurafenib between strains

The aim of this study was to assess the impact of P-gp and BCRP at the BBB on the intracranial efficacy of
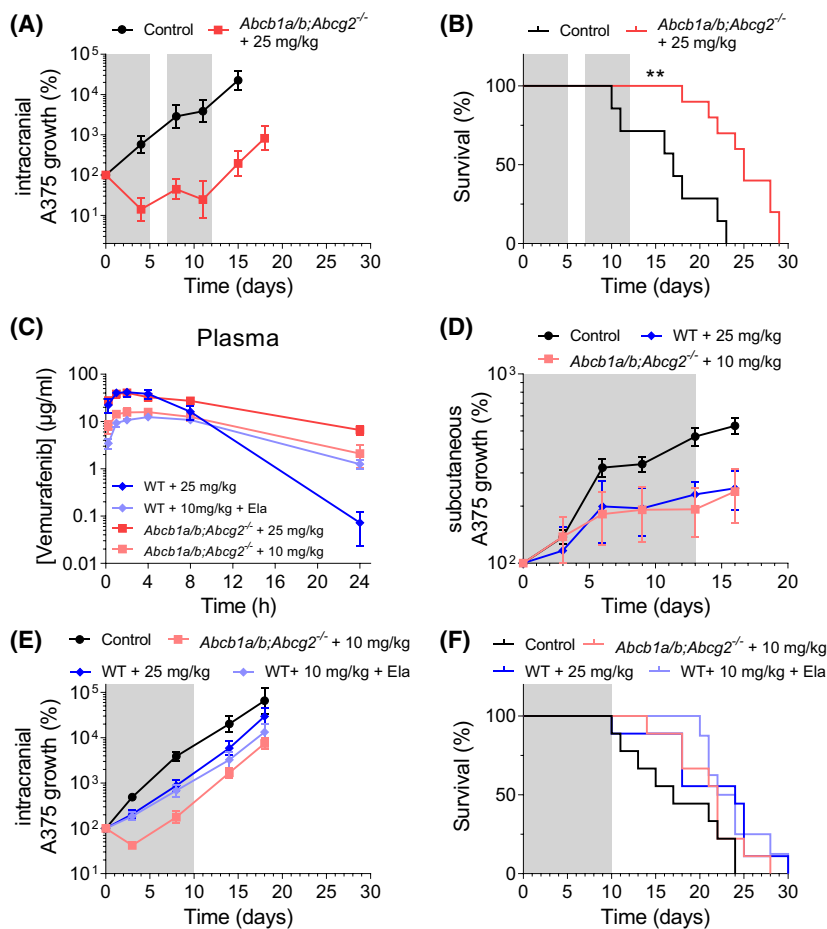
Fig. 2. Intrinsic and acquired resistance of A375 tumors against vemurafenib *in vivo*. (A) Tumor growth and (B) survival of *Abcb1a/b;Abcg2⁻/⁻* mice bearing intracranial A375 melanoma tumors treated with two rounds of 25 mg·kg⁻¹ vemurafenib q.d. × 5d or vehicle control. Treatment periods are shaded in gray. Data are represented as mean ± SE ($n \geq 7$); **$P < 0.01$. Statistically significant survival differences were determined using the log-rank test. (C) Oral vemurafenib plasma concentration–time curves in wild-type (WT) mice receiving 25 mg·kg⁻¹, WT mice receiving 10 mg·kg⁻¹ vemurafenib 4 h after administration of the P-glycoprotein (P-gp)/ breast cancer resistance protein (BCRP) inhibitor elacridar (Ela), *Abcb1a/b;Abcg2⁻/⁻* mice receiving 25 mg·kg⁻¹ vemurafenib and *Abcb1a/b;Abcg2⁻/⁻* mice receiving 10 mg·kg⁻¹ vemurafenib. Data are represented as mean ± SD ($n \geq 5$). (D) Tumor growth of subcutaneous A375 tumors grafted in WT or *Abcb1a/b;Abcg2⁻/⁻* mice treated with various doses of vemurafenib administered q.d. × 13d or vehicle control. Treatment period is shaded in gray. Data are represented as mean ± SE ($n \geq 7$). (E) Tumor growth and (F) survival of WT and *Abcb1a/b;Abcg2⁻/⁻* mice bearing intracranial A375 melanoma tumors treated with 25, 10, and 100 mg·kg⁻¹ elacridar (Ela) or 10 mg·kg⁻¹ vemurafenib q.d. × 10d or vehicle control. Treatment period is shaded in gray. Data are represented as mean ± SE ($n \geq 8$). Statistically significant survival differences were determined using the log-rank test. 5d, 5 days; 10d, 10 days; 13d, 13 days.

vemurafenib against MBMs by comparing WT and *Abcb1a/b;Abcg2⁻/⁻* mice. The systemic exposure and oral bioavailability of vemurafenib is known to be attenuated by P-gp and BCRP [18,19]. This difference in systemic exposure may confound a fair comparison between the strains and a reduction of the dose in *Abcb1a/b;Abcg2⁻/⁻* mice was deemed necessary. The previous pharmacokinetic studies were conducted in tumor-free mice and used different formulations than the Cremophor-based formulation utilized in this study. Therefore, we first assessed the plasma exposure in

tumor-free WT and *Abcb1a/b;Abcg2⁻/⁻* mice receiving vemurafenib in a Cremophor-based formulation. *Abcb1a/b;Abcg2⁻/⁻* mice received the same dose as WT mice (25 mg·kg⁻¹) or a reduced dose (10 mg·kg⁻¹). WT mice received the full dose (25 mg·kg⁻¹) or the reduced dose (10 mg·kg⁻¹) with concomitant administration of the P-gp/BCRP inhibitor elacridar (Fig. 2C). We administered vemurafenib 4 h after elacridar, as this is approximately the t_{max} of oral elacridar in mice. Similar to earlier studies, the plasma area under the curve (AUC) was significantly higher in *Abcb1a/b;Abcg2⁻/⁻* mice

compared with WT mice receiving the same dose (Table 1). Notably, the terminal half-life of vemurafenib was considerably shorter in WT mice, making accurate leveling between strains by dose adjustments difficult. Reducing the dose to 10 mg·kg^{-1} in *Abcb1a/b;Abcg2*$^{-/-}$ mice resulted in a lower plasma AUC than WT at 25 mg·kg^{-1}, but the trough levels were significantly higher. Co-administration of elacridar to WT mice yielded a vemurafenib plasma exposure similar to that in *Abcb1a/b;Abcg2*$^{-/-}$ mice, suggesting that elacridar efficiently inhibits systemic clearance mediated by P-gp and BCRP.

In order to assess whether the dose leveling between the strains was appropriate, we treated subcutaneously grafted A375 tumors with 25 mg·kg^{-1} vemurafenib in WT mice and 10 mg·kg^{-1} vemurafenib in *Abcb1a/b; Abcg2*$^{-/-}$ mice for 13 consecutive days. Vemurafenib penetration into subcutaneous tumors is similar in WT and *Abcb1a/b;Abcg2*$^{-/-}$ mice and as we found that vemurafenib was equally effective (Fig. 2D) and did not result in body weight loss (Fig. S1B), we selected these dose regimens for the efficacy study against intracranial A375 tumors.

P-gp and BCRP limit vemurafenib efficacy against intracranial tumors

We next grafted WT and *Abcb1a/b;Abcg2*$^{-/-}$ mice with intracranial A375 tumors, to study whether P-gp and BCRP at the BBB affect antitumor efficacy in an MBM model. We again treated WT mice with 25 mg·kg^{-1} and used 10 mg·kg^{-1} vemurafenib for *Abcb1a/b;Abcg2*$^{-/-}$ mice. We also added a group of WT mice receiving 10 mg·kg^{-1} with concomitant elacridar. In this case, we now found that vemurafenib was more effective in *Abcb1a/b;Abcg2*$^{-/-}$ than in WT mice (Fig. 2E). Again, we could not observe any weight loss induced by any treatment regimen (Fig. S1C). While vemurafenib only reduced A375 growth speed in WT mice, it induced tumor regression in *Abcb1a/b; Abcg2*$^{-/-}$ mice during the first 3 days of treatment. Notably, however, while still under therapy, regrowth occurred in these mice reaching a similar tumor growth speed as in untreated animals before the completion of treatment. As a result, survival was not significantly extended (Fig. 2F). Pharmacological inhibition of P-gp and BCRP by elacridar was less efficacious, as the vemurafenib antitumor efficacy was greater in *Abcb1a/ b;Abcg2*$^{-/-}$ mice receiving 10 mg·kg^{-1} than in WT mice receiving elacridar and the same dose of vemurafenib (Fig. 2E). Taken together, these data indicate that P-gp and BCRP at the BBB can diminish the efficacy of vemurafenib against MBMs.

P-gp and BCRP reduce vemurafenib penetration in MBMs

P-gp and BCRP limit the brain penetration of vemurafenib by virtue of their efflux function at the BBB [18,19]. However, it is unknown whether the penetration into MBMs is similarly affected, as these lesions display signs of a compromised BBB on contrast-enhanced MRI. We therefore measured the vemurafenib distribution in tumor-bearing WT and *Abcb1a/b; Abcg2*$^{-/-}$ mice after three daily administrations of vemurafenib. We collected brain, tumor, and plasma samples at approximately the t_{max} of vemurafenib (4 h after the last administration). The vemurafenib plasma concentration in WT mice receiving 25 mg·kg^{-1} was around one-fourth of the concentration observed in our previous pharmacokinetic experiment (Figs 2C and 3A), whereas much smaller discrepancies were observed in *Abcb1a/b;Abcg2*$^{-/-}$ mice (twofold) and WT mice that also received elacridar (no difference). Notably, these tumor-bearing mice in the later experiment received three administrations of vemurafenib and the tumor-free mice in the earlier experiment only one. Therefore, these data could suggest induction of P-gp and BCRP by repeated vemurafenib administration, resulting in increased clearance.

The apparent discrepancies in plasma concentration do not affect the results of the brain penetration as we always assess tissue–plasma ratio within each mouse. The vemurafenib concentrations in different brain regions differed greatly among all treatment groups (Fig. 3B). As expected, the highest concentrations were reached in *Abcb1a/b;Abcg2*$^{-/-}$ mice receiving 25 mg·kg^{-1} vemurafenib. The concentrations were lower in *Abcb1a/b;Abcg2*$^{-/-}$ mice receiving 10 mg·kg^{-1} vemurafenib, but this was only a result of the lower dose, as tissue–plasma ratios were similar between both dose levels in *Abcb1a/b;Abcg2*$^{-/-}$ mice (Fig. 3C). In line with previous reports, the vemurafenib penetration in normal brain regions of WT mice was negligible. The tissue–plasma ratios were very close to the total blood volume of the murine brain (approximately 2%). Elacridar increased the vemurafenib concentration in healthy brain regions, but inhibition of P-gp and BCRP was incomplete, since the levels and brain-to-plasma ratios were significantly lower than in *Abcb1a/b;Abcg2*$^{-/-}$ mice. Vemurafenib penetrated into the tumor core in WT mice, but the levels were approximately half of those achieved in *Abcb1a/b; Abcg2*$^{-/-}$ mice. Elacridar was also not able to improve the penetration of vemurafenib into the tumor core to the same level as in *Abcb1a/b;Abcg2*$^{-/-}$ mice. These data show that P-gp and BCRP can still limit

Table 1. Pharmacokinetic parameters of vemurafenib after oral administration of different doses to wild-type (WT) and $Abcb1a/b;Abcg2^{-/-}$ FVB mice. AUC, area under the curve; C_{max}, maximum concentration in plasma; CL/F, apparent clearance after oral administration; $t_{1/2}$, elimination half-life; t_{max}, time to reach maximum plasma concentration. Data are represented as mean ± SD ($n \geq 5$).

Parameter	Time (h)	WT, 25 mg·kg^{-1}	$Abcb1a/b;Abcg2^{-/-}$, 25 mg·kg^{-1}	WT, 10 mg·kg^{-1} + elacridar	$Abcb1a/b;Abcg2^{-/-}$, 10 mg·kg^{-1}
AUC$_{plasma}$, µg·(mL·h)$^{-1}$	0–4	147 ± 28	140 ± 16	38 ± 5.7	56 ± 7.2*
AUC$_{plasma}$, µg·(mL·h)$^{-1}$	0–24	390 ± 98	530 ± 68*	180 ± 24	230 ± 35
AUC$_{plasma}$, µg·(mL·h)$^{-1}$	0–∞	390 ± 99	610 ± 84**	190 ± 23	250 ± 49
C_{max}, µg·mL^{-1}		42 ± 7.7	41 ± 4.5	12 ± 1.7	17 ± 1.7*
t_{max}, h		2.6 ± 1.3	1.9 ± 0.9	3.6 ± 0.9	2.8 ± 1.1
$t_{1/2}$, h		2.1 ± 0.2	8.5 ± 1.2****	5.8 ± 0.6	6.7 ± 1.4
CL/F, L·(kg·h)$^{-1}$		0.07 ± 0.017	0.04 ± 0.006**	0.05 ± 0.006	0.04 ± 0.006

*$P < 0.05$, **$P < 0.01$, ****$P < 0.0001$, compared with WT mice receiving the same vemurafenib dose. Differences were analyzed by one-way ANOVA followed by Bonferroni *post hoc* tests.
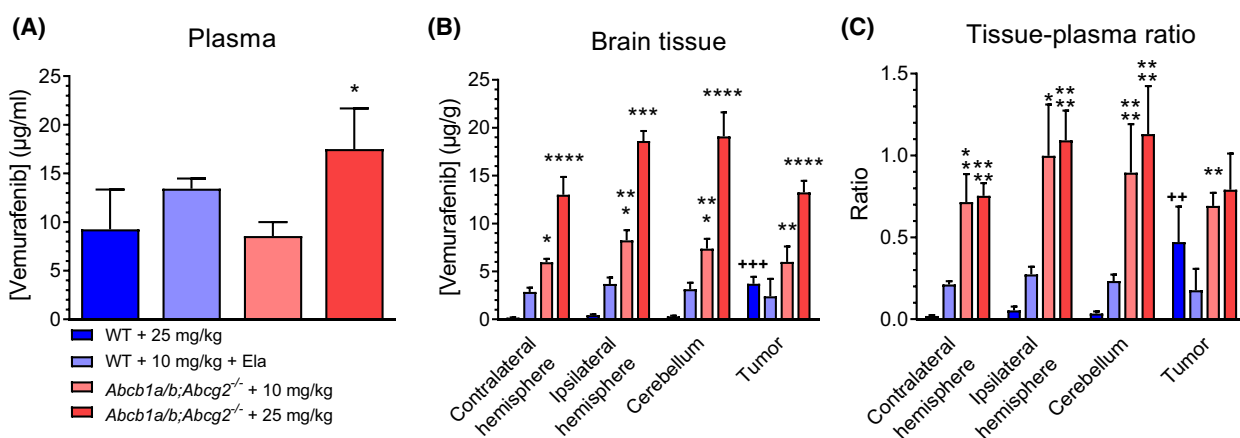

Fig. 3. Vemurafenib concentrations in tumor and healthy brain of wild-type (WT) and $Abcb1a/b;Abcg2^{-/-}$ mice. (A) Plasma concentrations, (B) brain tissue concentrations, and (C) tissue–plasma ratios in WT and $Abcb1a/b;Abcg2^{-/-}$ mice 4 h after receiving oral vemurafenib at doses of 25, 10, or 10 mg·kg^{-1} 4 h after receiving 100 mg·kg^{-1} oral elacridar (Ela). The contralateral hemisphere represents the tumor-free hemisphere. The ipsilateral hemisphere is the hemisphere where the tumor was injected, from which all macroscopic tumor was removed. Data are represented as mean ± SD ($n \geq 3$); *$P < 0.05$, **$P < 0.01$, ***$P < 0.001$, ****$P < 0.0001$, compared with WT mice receiving 25 mg·kg^{-1} vemurafenib; $^{++}P < 0.01$, $^{+++}P < 0.001$, compared with the contralateral hemisphere level of the same group. Differences were analyzed by one-way ANOVA followed by Bonferroni *post hoc* tests.

vemurafenib penetration into MBMs, even when the tumor lesion has compromised BBB integrity. These drug distribution data are in line with the observed intracranial antitumor efficacy (Fig. 2A,E), as vemurafenib tumor concentrations were similar between WT mice receiving 25 mg·kg^{-1} and WT mice receiving 10 mg·kg^{-1} of vemurafenib with concomitant elacridar, but lower than in $Abcb1a/b;Abcg2^{-/-}$ mice receiving 10 or 25 mg·kg^{-1} vemurafenib.

Intracranial A375 tumors develop therapy resistance despite sufficient vemurafenib tumor penetration and target inhibition

As mentioned above, the A375 MBM model is responsive to vemurafenib, but developed therapy resistance

after just a few days of treatment in $Abcb1a/b;Abcg2^{-/-}$ mice receiving 10 mg·kg^{-1} vemurafenib (Fig. 2E). Since P-gp and BCRP are absent in these mice, we reasoned that P-gp/BCRP-unrelated pharmacokinetic phenomena may underlie the observed resistance. For instance, induction of vemurafenib presystemic metabolism, systemic clearance, or efflux at the BBB by other ABC transporters might result in diminished vemurafenib brain concentrations after repeated administrations. However, the vemurafenib concentrations in various brain regions in tumor-bearing mice treated for a short (5 days) or long (10 days) period were not different in $Abcb1a/b;Abcg2^{-/-}$ mice and WT mice also receiving elacridar (Fig. 4A–D). In fact, in contrast to the observed antitumor efficacy at 5 and 10 days of treatment (Fig. 2E), the vemurafenib
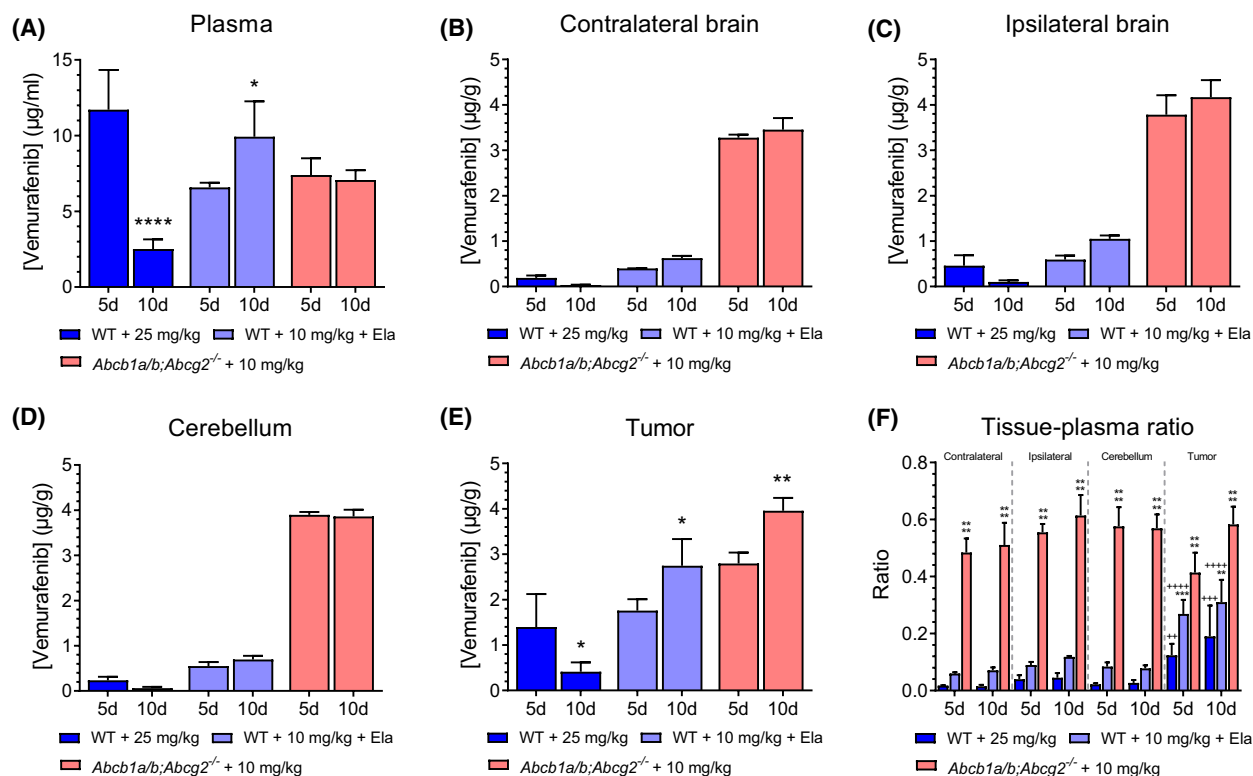
Fig. 4. Vemurafenib concentrations in short-term and long-term treated intracranial A375 tumors. Vemurafenib concentrations in (A) plasma, (B) contralateral brain, (C) ipsilateral brain, (D) cerebellum, and (E) tumor after short-term (5 days; 5d) and long-term treatment (10 days; 10d) of A375 melanomas brain metastases. Tumor-bearing wild-type (WT) or *Abcb1a/b;Abcg2$^{-/-}$* mice orally received 25, 10 or 10 mg·kg^{-1} vemurafenib, and 100 mg·kg^{-1} oral elacridar (Ela). Data are represented as mean ± SD ($n \geq 3$); *$P < 0.05$, **$P < 0.01$, ****$P < 0.0001$, compared with short-term treated tumors of the same group. Differences were analyzed by one-way ANOVA followed by Bonferroni *post hoc* tests. (F) Vemurafenib tissue–plasma ratios for different brain regions in 5 and 10 day-treated tumors. Data are represented as mean ± SD ($n \geq 3$); **$P < 0.01$, ***$P < 0.001$, ****$P < 0.0001$, compared with WT animals treated with 25 mg·kg^{-1} vemurafenib; $^{++}P < 0.01$, $^{+++}P < 0.001$, $^{++++}P < 0.0001$, compared with the contralateral hemisphere region within the same treatment group. Differences were analyzed by one-way ANOVA followed by Bonferroni *post hoc* tests.

concentration in the tumor regions of these mice was even higher at the later time point (Fig. 4E). Notably, we did find a considerably lower vemurafenib concentration in plasma in long-term treated WT mice compared with short-term treated WT mice (Fig. 4A). Brain and tumor concentrations were also lower as a consequence of the lower plasma concentration, as the tissue–plasma ratios were unchanged over time (Fig. 4F). Again, we found no reduction in vemurafenib plasma concentration in *Abcb1a/b;Abcg2$^{-/-}$* mice or WT mice also receiving elacridar, indicating that the reduction in vemurafenib concentration over time in WT mice was mediated by P-gp and/or BCRP.

Since the vemurafenib concentration in responsive short-term (5 days) treated tumors and resistant long-term (10 days) treated tumors was similar, we explored alternative ways by which intracranial A375 tumor may acquire resistance in a small pilot cohort we had available for immunohistochemical analysis ($n = 2$ per

group). Even though the cohort sample size was too small to robustly detect subtle differences in expression and therefore conduct quantitative analyses, we expected that we would be able to qualitatively observe whether any substantial biological effects occurred. For instance, we observed canonical pathway inhibition in vemurafenib-resistant MBMs, as indicated by the profoundly reduced immunohistochemical staining of downstream BRAF^{V600E} targets phospho-S6 and phospho-4EBP1 (Fig. 5). BRAF^{V600E}, phospho-ERK, and phospho-AKT were still low or unaffected, suggesting that resistance occurred via noncanonical growth signaling, as the proliferation marker Ki-67 was similarly unaffected. Upstream growth factor receptors are likely candidates for such a mechanism and have been demonstrated to mediate resistance to BRAF^{V600} inhibitors before [31–34]. However, PDGFRβ, AXL, NGFR, MET, and EGFR expression did not seem to be increased in resistant
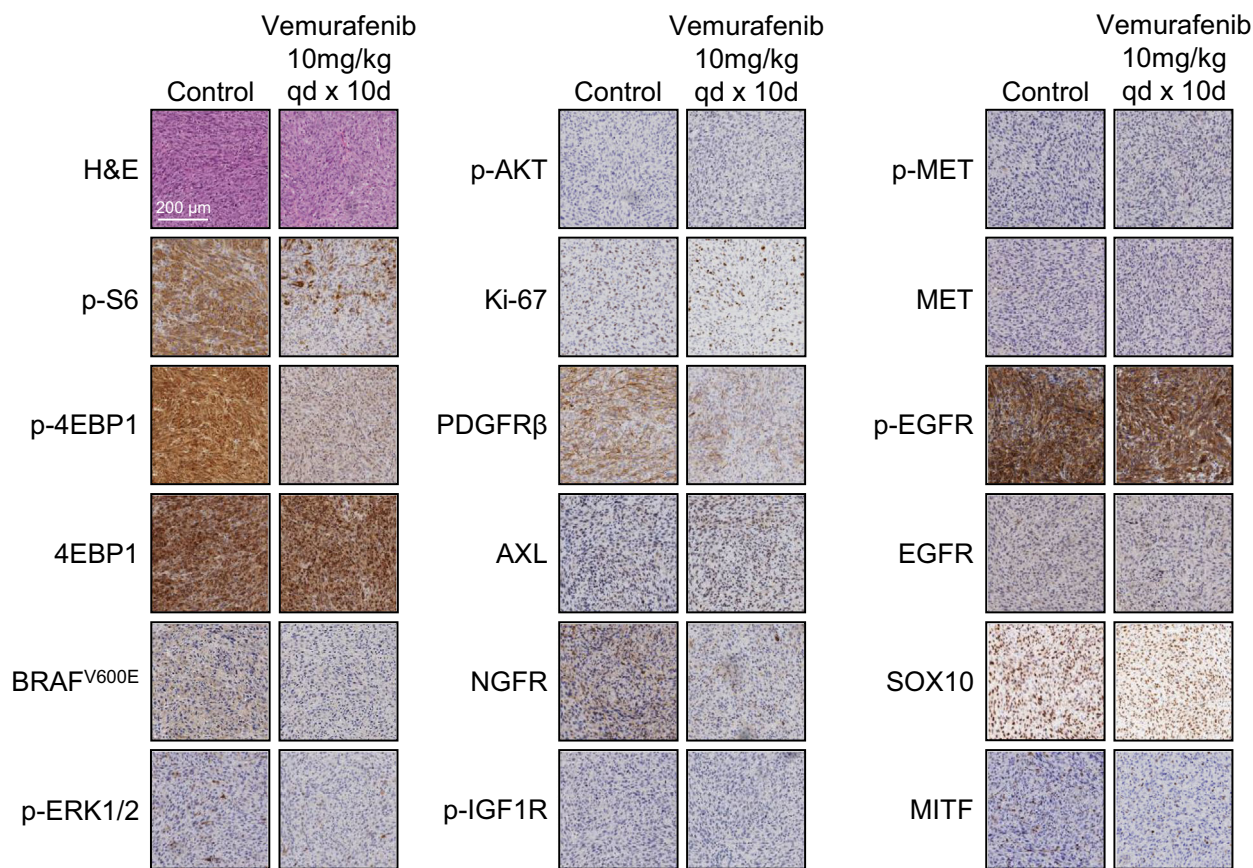
Fig. 5. Immunohistochemical analysis of vemurafenib-resistant A375 melanoma brain metastases. Tumors growing in *Abcb1a/b;Abcg2*$^{-/-}$ mice treated orally with 10 mg·kg^{-1} vemurafenib × 10d (resistant stage) were stained for various markers and compared with untreated tumors. Scale bar represents 200 μm. AXL, tyrosine-protein kinase receptor UFO; H&E, hematoxylin and eosin; Ki-67, proliferation marker protein Ki-67; MITF, microphtalmia transcription factor; NGFR, neural growth factor receptor; p-4EBP1, phospho-eukaryotic translation initiation factor 4E-binding protein 1; p-AKT, phospho-AKT; PDGFRβ, platelet-derived growth factor receptor β; p-EGFR, phospho-epidermal growth factor receptor; p-ERK, phospho-extracellular single-regulated kinase; p-IGF1R, phospho-insulin-like growth factor 1 receptor; p-MET, phospho-MET; p-S6, phospho-ribosomal protein S6; SOX10, sex-determining region Y-box 10. 10d, 10 days.

tumors and neither was signaling through phospho-IGF1R, phospho-MET or phospho-EGFR. In fact, PDGFRβ expression appeared to be diminished by vemurafenib treatment. Furthermore, we could not detect large differences in expression of transcription factors that have been implicated in acquired resistance mechanisms such as SOX10 [33] and MITF [31]. Taken together, these findings suggest that rapid resistance in intracranial A375 tumors does not occur via pharmacological processes but through acquiring previously unreported noncanonical growth signaling.

Discussion

The introduction of BRAF and MEK inhibitors has dramatically improved the survival of metastatic melanoma patients. However, clinical responses in MBMs are less durable than those in extracranial metastases, suggesting MBMs may be intrinsically resistant to therapy [16]. By using a preclinical mouse model, we here show that although BRAF^{V600E}-positive MBMs cause a disruption of BBB integrity, P-gp and BCRP are expressed in the tumor blood vessels, thereby reducing the efficacy of vemurafenib by limiting its distribution into MBM lesions. Furthermore, by using *Abcb1a/b;Abcg2*$^{-/-}$ mice we found that BRAF^{V600E}-positive MBMs are initially responsive to vemurafenib in the absence of P-gp and BCRP. However, they rapidly acquire resistance in the brains of these mice. This acquired resistance is not due to reduced levels of vemurafenib in the tumor, also not after repeated exposure. Therefore, BRAF^{V600E}-positive MBMs must acquire resistance to therapy by resorting to noncanonical proliferation signaling. However, no evidence was found that

this occurs via previously described resistance mechanisms in extracranial melanomas [31–34].

The BBB limits the brain penetration and antitumor efficacy of treatment for primary brain tumors such as glioblastoma and diffuse intrinsic pontine glioma [35]. However, its impact on the treatment of brain metastases is less well established [36]. Brain metastases usually demonstrate contrast enhancement on T1-weighted MR imaging, indicating a loss of BBB integrity. Moreover, MBMs grow as relatively circumscribed lesions without much invasion of surrounding brain and remain in the vicinity of the vasculature [37,38]. Consequently, MBM cells are rarely found outside of the contrast-enhanced brain regions where the BBB is intact. Therefore, clinical responses can be observed with poorly brain-penetrable drugs such as vemurafenib. These responses lead some to conclude that the relevance of the BBB is limited in brain metastases. Contrast enhancement on MR images indeed indicates a physical disruption of the BBB integrity, as tight junctions normally prevent paracellular diffusion of contrast agents. However, despite this loss of integrity, the drug efflux transporters P-gp and BCRP can still be functional in these brain lesions [26]. In line with this hypothesis, we observed increased efficacy of vemurafenib against a BRAF^{V600E}-positive MBM model that displays T1-weighted MRI contrast enhancement when these tumors were grafted in $Abcb1a/b;Abcg2^{-/-}$ mice and when vemurafenib was combined with the P-gp/BCRP inhibitor elacridar in WT mice. Hereby, we showed that even when BBB integrity is lost, brain penetration and antitumor efficacy of targeted agents that are substrates of P-gp and/or BCRP can still be limited.

The BBB may thus limit the efficacy of BRAF inhibitors against BRAF-mutated tumors residing in the brain. These do not only include brain metastases of melanoma [39] and nonsmall cell lung cancer [40], but also subsets of several different of primary adult [41] and pediatric [42] brain tumors. The expression of P-gp and BCRP in vessels of primary brain tumors is well-documented [35,43]. Unfortunately, there are only two papers on P-gp or BCRP expression in blood vessels of brain metastatic lesions. Richtig *et al.* [44] reported a general lack of P-gp expression in MBMs, whereas the blood vessels of various subtypes of breast cancer brain metastases were positive for BCRP [45]. The results in human MBMs are not in line with our results in mice. This may be related to the size of the lesion, as stainings in human samples were all done on relatively large lesions that may depend more on angiogenesis. Notably, BCRP may be a more important drug efflux transporter in humans than in mice, since it is more abundantly expressed [46].

To maximize the potential of BRAF inhibitor therapy against intracranial malignancies, it is important to optimize its pharmakinetic and pharmacodynamic parameters. In that regard, vemurafenib does not appear to be the superior BRAF inhibitor. Pharmacokinetically, the brain–plasma ratios of oral vemurafenib in WT mice are around 0.02 [18,19], for encorafenib roughly 0.004 [21] and for dabrafenib approximately 0.1 [20]. While a brain–plasma ratio of 0.1 for dabrafenib is still quite poor, it is clearly better than those of vemurafenib and encorafenib. Dabrafenib is also pharmacodynamically superior, as its IC$_{50}$ against A375 cells is 4 nM [47]. Encorafenib is similary potent against A375 cells (IC$_{50}$ = 4 nM), but the IC$_{50}$ of vemurafenib is approximately 100-fold higher at rougly 500 nM [48,49]. As a consequence of the higher potency, plasma levels of dabrafenib given at therapeutic doses are about 20- to 50-fold lower [50]. Nevertheless, these data suggest that dabrafenib may be the inhibitor of choice for treatment of BRAF-mutated intracranial tumors. This notion seems to be supported by clinical data. MBM patients receiving vemurafenib had a median overall survival of 4.3 months [51], compared with 7 months for dabrafenib treatment alone [16]. To what extent this superior overall survival can be attributed to the higher intrinsic potency of dabrafenib and how much to its higher brain penetration is unclear, but both characteristics are likely to have contributed. In summary, the currently available data seems to suggest that dabrafenib-based treatment regimens have superior efficacy and that co-adminstration of P-gp/BCRP inhibitors such as elacridar may further enhance their efficacy.

Next to reduced sensitivity caused by the BBB, we observed a striking development of acquired resistance that occurred much more rapidly than is typically reported for extracranial tumor models [52]. Interestingly, these data seem to be in line with observations in metastastatic melanoma patients. In a phase II study investigating dabrafenib and trametinib combination therapy in metastatic melonoma patients with brain metastases, similar intracranial and extracranial response rates (approximately 50%) were observed [17]. However, the duration of response was considerably shorter for intracranial metastases (6.5 months) than for extracranial metastases (10.2 months). The reason why MBMs acquire therapy resistance more rapidly is not yet understood. Several resistance mechanisms to BRAF inhibitors have been described to date [53]. Notable mechanisms include increased EGFR signaling [33], increased PDGFRβ signaling [32] and a low MITF/AXL ratio [31]. The previously reported effect sizes of these mechanisms are quite striking and since

we could not detect any major changes in our pilot cohort of resistant intracranial A375 tumors these mechanisms appear not be implicated in the resistance we observed (Fig. 5). A very recently discovered resistance mechanism is the acquisition of a secondary *BRAF* mutation resulting in a BRAF$^{V600E/L514V}$ oncoprotein [54], but this is unlikely to occur in our A375 MBM model as this mutation would lead to increased canonical MAPK pathway signaling, which we did not observe. Microenvironment-related resistance mechanisms exerted by reactive astrocytes have also been proposed [37]. For instance, factors secreted by astrocytes have been demonstrated to increase AKT signaling in melanoma cells *in vitro* [55]. This specific mechanism is unlikely to have occurred in our study, as we did not observed increased p-AKT levels in resistant tumors (Fig. 5). However, it does indicate that the microenvironment can contribute to acquired therapy resistance. Indeed, a potential role for the MBM microenvironment may also help to explain the observed differential clinical responses of intracranial and extracranial metastases [17].

Taken together, this study demonstrates that BRAF^{V600E}-positive MBMs are not only less sensitive to vemurafenib because they are still partially protected by expression of P-gp and BCRP in the disrupted BBB, but they can also rapidly acquire resistance likely dependent on the unique microenvironment of the brain. Adding a P-gp/BCRP inhibitor to BRAF inhibitor therapy may therefore improve survival by overcoming intrinsic resistance of MBMs. However, understanding the mechanism behind the apparent brain-specific acquired resistance will likely be necessary to induce long-term responses.

Acknowledgements

Conflict of interest

The authors declare no conflict of interest.

Peer review

The peer review history for this article is available at https://www.webofscience.com/api/gateway/wos/peer-review/10.1002/2211-5463.13730.

Data accessibility

The datasets generated during and/or analyzed during the current study are available from the corresponding author upon reasonable request.

Author contributions

JHB, OvT, and MCdG conceived the study. PZ, LEK, LCMB, SF, and MCdG collected and analyzed data. JHB, OvT, and MCdG supervised the study. OvT and MCdG wrote the manuscript with input from all authors.

References

1 Sloot S, Chen YA, Zhao X, Weber JL, Benedict JJ, Mulé JJ, Smalley KS, Weber JS, Zager JS, Forsyth PA *et al.* (2018) Improved survival of patients with melanoma brain metastases in the era of targeted BRAF and immune checkpoint therapies. *Cancer* **124**, 297–305.

2 Davies H, Bignell GR, Cox C, Stephens P, Edkins S, Clegg S, Teague J, Woffendin H, Garnett MJ, Bottomley W *et al.* (2002) Mutations of the BRAF gene in human cancer. *Nature* **417**, 949–954.

3 Hodis E, Watson IR, Kryukov GV, Arold ST, Imielinski M, Theurillat JP, Nickerson E, Auclair D, Li L, Place C *et al.* (2012) A landscape of driver mutations in melanoma. *Cell* **150**, 251–263.

4 Kim G, McKee AE, Ning YM, Hazarika M, Theoret M, Johnson JR, Xu QC, Tang S, Sridhara R, Jiang X *et al.* (2014) FDA approval summary: vemurafenib for treatment of unresectable or metastatic melanoma with the BRAFV600E mutation. *Clin Cancer Res* **20**, 4994–5000.

5 Ballantyne AD and Garnock-Jones KP (2013) Dabrafenib: first global approval. *Drugs* **73**, 1367–1376.

6 Shirley M (2018) Encorafenib and binimetinib: first global approvals. *Drugs* **78**, 1277–1284.

7 Chapman PB, Hauschild A, Robert C, Haanen JB, Ascierto P, Larkin J, Dummer R, Garbe C, Testori A, Maio M *et al.* (2011) Improved survival with vemurafenib in melanoma with BRAF V600E mutation. *N Engl J Med* **364**, 2507–2516.

8 Hauschild A, Grob JJ, Demidov LV, Jouary T, Gutzmer R, Millward M, Rutkowski P, Blank CU, Miller WH Jr, Kaempgen E *et al.* (2012) Dabrafenib in BRAF-mutated metastatic melanoma: a multicentre, open-label, phase 3 randomised controlled trial. *Lancet* **380**, 358–365.

9 Delord JP, Robert C, Nyakas M, McArthur GA, Kudchakar R, Mahipal A, Yamada Y, Sullivan R, Arance A, Kefford RF *et al.* (2017) Phase I dose-escalation and -expansion study of the BRAF inhibitor encorafenib (LGX818) in metastatic BRAF-mutant melanoma. *Clin Cancer Res* **23**, 5339–5348.

10 Van Allen EM, Wagle N, Sucker A, Treacy DJ, Johannessen CM, Goetz EM, Place CS, Taylor-Weiner A, Whittaker S, Kryukov GV *et al.* (2014) The genetic landscape of clinical resistance to RAF inhibition in metastatic melanoma. *Cancer Discov* **4**, 94–109.

11 Signorelli J and Shah Gandhi A (2017) Cobimetinib. *Ann Pharmacother* **51**, 146–153.

12 Odogwu L, Mathieu L, Blumenthal G, Larkins E, Goldberg KB, Griffin N, Bijwaard K, Lee EY, Philip R, Jiang X *et al.* (2018) FDA approval summary: dabrafenib and trametinib for the treatment of metastatic non-small cell lung cancers harboring BRAF V600E mutations. *Oncologist* **23**, 740–745.

13 Dummer R, Ascierto PA, Gogas HJ, Arance A, Mandala M, Liszkay G, Garbe C, Schadendorf D, Krajsova I, Gutzmer R *et al.* (2018) Encorafenib plus binimetinib versus vemurafenib or encorafenib in patients with BRAF-mutant melanoma (COLUMBUS): a multicentre, open-label, randomised phase 3 trial. *Lancet Oncol* **19**, 603–615.

14 Ascierto PA, McArthur GA, Dreno B, Atkinson V, Liszkay G, Di Giacomo AM, Mandala M, Demidov L, Stroyakovskiy D, Thomas L *et al.* (2016) Cobimetinib combined with vemurafenib in advanced BRAF(V600)-mutant melanoma (coBRIM): updated efficacy results from a randomised, double-blind, phase 3 trial. *Lancet Oncol* **17**, 1248–1260.

15 Long GV, Stroyakovskiy D, Gogas H, Levchenko E, de Braud F, Larkin J, Garbe C, Jouary T, Hauschild A, Grob JJ *et al.* (2015) Dabrafenib and trametinib versus dabrafenib and placebo for Val600 BRAF-mutant melanoma: a multicentre, double-blind, phase 3 randomised controlled trial. *Lancet* **386**, 444–451.

16 Long GV, Trefzer U, Davies MA, Kefford RF, Ascierto PA, Chapman PB, Puzanov I, Hauschild A, Robert C, Algazi A *et al.* (2012) Dabrafenib in patients with Val600Glu or Val600Lys BRAF-mutant melanoma metastatic to the brain (BREAK-MB): a multicentre, open-label, phase 2 trial. *Lancet Oncol* **13**, 1087–1095.

17 Davies MA, Saiag P, Robert C, Grob JJ, Flaherty KT, Arance A, Chiarion-Sileni V, Thomas L, Lesimple T, Mortier L *et al.* (2017) Dabrafenib plus trametinib in patients with BRAF(V600)-mutant melanoma brain metastases (COMBI-MB): a multicentre, multicohort, open-label, phase 2 trial. *Lancet Oncol* **18**, 863–873.

18 Durmus S, Sparidans RW, Wagenaar E, Beijnen JH and Schinkel AH (2012) Oral availability and brain penetration of the B-RAFV600E inhibitor vemurafenib can be enhanced by the P-glycoprotein (ABCB1) and breast cancer resistance protein (ABCG2) inhibitor elacridar. *Mol Pharm* **9**, 3236–3245.

19 Mittapalli RK, Vaidhyanathan S, Sane R and Elmquist WF (2012) Impact of P-glycoprotein (ABCB1) and breast cancer resistance protein (ABCG2) on the brain distribution of a novel BRAF inhibitor: vemurafenib (PLX4032). *J Pharmacol Exp Ther* **342**, 33–40.

20 Mittapalli RK, Vaidhyanathan S, Dudek AZ and Elmquist WF (2013) Mechanisms limiting distribution of the threonine-protein kinase B-RaF(V600E) inhibitor dabrafenib to the brain: implications for the treatment of melanoma brain metastases. *J Pharmacol Exp Ther* **344**, 655–664.

21 Wang J, Gan C, Sparidans RW, Wagenaar E, van Hoppe S, Beijnen JH and Schinkel AH (2018) P-glycoprotein (MDR1/ABCB1) and breast cancer resistance protein (BCRP/ABCG2) affect brain accumulation and intestinal disposition of encorafenib in mice. *Pharmacol Res* **129**, 414–423.

22 Sakji-Dupre L, Le Rhun E, Templier C, Desmedt E, Blanchet B and Mortier L (2015) Cerebrospinal fluid concentrations of vemurafenib in patients treated for brain metastatic BRAF-V600 mutated melanoma. *Melanoma Res* **25**, 302–305.

23 Durmus S, Hendrikx JJ and Schinkel AH (2015) Apical ABC transporters and cancer chemotherapeutic drug disposition. *Adv Cancer Res* **125**, 1–41.

24 de Gooijer MC, de Vries NA, Buckle T, Buil LCM, Beijnen JH, Boogerd W and van Tellingen O (2018) Improved brain penetration and antitumor efficacy of temozolomide by inhibition of ABCB1 and ABCG2. *Neoplasia* **20**, 710–720.

25 Kim M, Ma DJ, Calligaris D, Zhang S, Feathers RW, Vaubel RA, Meaux I, Mladek AC, Parrish KE, Jin F *et al.* (2018) Efficacy of the MDM2 inhibitor SAR405838 in glioblastoma is limited by poor distribution across the blood-brain barrier. *Mol Cancer Ther* **17**, 1893–1901.

26 de Gooijer MC, Kemper EM, Buil LCM, Citirikkaya CH, Buckle T, Beijnen JH and van Tellingen O (2021) ATP binding cassette transporters restrict drug delivery and efficacy against brain tumors even when blood-brain barrier integrity is lost. *Cell Rep Med* **2**, 100184.

27 Schackert G and Fidler IJ (1988) Development of in vivo models for studies of brain metastasis. *Int J Cancer* **41**, 589–594.

28 Schindelin J, Arganda-Carreras I, Frise E, Kaynig V, Longair M, Pietzsch T, Preibisch S, Rueden C, Saalfeld S, Schmid B *et al.* (2012) Fiji: an open-source platform for biological-image analysis. *Nat Methods* **9**, 676–682.

29 Smalley I, Chen Z, Phadke M, Li J, Yu X, Wyatt C, Evernden B, Messina JL, Sarnaik A, Sondak VK *et al.* (2021) Single-cell characterization of the immune microenvironment of melanoma brain and leptomeningeal metastases. *Clin Cancer Res* **27**, 4109–4125.

30 Zhang Y, Huo M, Zhou J and Xie S (2010) PKSolver: an add-in program for pharmacokinetic and pharmacodynamic data analysis in Microsoft excel. *Comput Methods Programs Biomed* **99**, 306–314.

31 Sun C, Wang L, Huang S, Heynen GJ, Prahallad A, Robert C, Haanen J, Blank C, Wesseling J, Willems SM *et al.* (2014) Reversible and adaptive resistance to BRAF(V600E) inhibition in melanoma. *Nature* **508**, 118–122.

32 Nazarian R, Shi H, Wang Q, Kong X, Koya RC, Lee H, Chen Z, Lee MK, Attar N, Sazegar H *et al.* (2010) Melanomas acquire resistance to B-RAF(V600E) inhibition by RTK or N-RAS upregulation. *Nature* **468**, 973–977.

33 Muller J, Krijgsman O, Tsoi J, Robert L, Hugo W, Song C, Kong X, Possik PA, Cornelissen-Steijger PD, Geukes Foppen MH *et al.* (2014) Low MITF/AXL ratio predicts early resistance to multiple targeted drugs in melanoma. *Nat Commun* **5**, 5712.

34 Wang L, Leite de Oliveira R, Huijberts S, Bosdriesz E, Pencheva N, Brunen D, Bosma A, Song JY, Zevenhoven J, Los-de Vries GT *et al.* (2018) An acquired vulnerability of drug-resistant melanoma with therapeutic potential. *Cell* **173**, 1413–1425.e1414.

35 van Tellingen O, Yetkin-Arik B, de Gooijer MC, Wesseling P, Wurdinger T and de Vries HE (2015) Overcoming the blood-brain tumor barrier for effective glioblastoma treatment. *Drug Resist Updat* **19**, 1–12.

36 Gampa G, Vaidhyanathan S, Sarkaria JN and Elmquist WF (2017) Drug delivery to melanoma brain metastases: can current challenges lead to new opportunities? *Pharmacol Res* **123**, 10–25.

37 Preusser M, Capper D, Ilhan-Mutlu A, Berghoff AS, Birner P, Bartsch R, Marosi C, Zielinski C, Mehta MP, Winkler F *et al.* (2012) Brain metastases: pathobiology and emerging targeted therapies. *Acta Neuropathol* **123**, 205–222.

38 Fidler IJ (2011) The role of the organ microenvironment in brain metastasis. *Semin Cancer Biol* **21**, 107–112.

39 Capper D, Berghoff AS, Magerle M, Ilhan A, Wohrer A, Hackl M, Pichler J, Pusch S, Meyer J, Habel A *et al.* (2012) Immunohistochemical testing of BRAF V600E status in 1,120 tumor tissue samples of patients with brain metastases. *Acta Neuropathol* **123**, 223–233.

40 Dagogo-Jack I, Martinez P, Yeap BY, Ambrogio C, Ferris LA, Lydon C, Nguyen T, Jessop NA, Iafrate AJ, Johnson BE *et al.* (2019) Impact of BRAF mutation class on disease characteristics and clinical outcomes in BRAF-mutant lung cancer. *Clin Cancer Res* **25**, 158–165.

41 Behling F, Barrantes-Freer A, Skardelly M, Nieser M, Christians A, Stockhammer F, Rohde V, Tatagiba M, Hartmann C, Stadelmann C *et al.* (2016) Frequency of BRAF V600E mutations in 969 central nervous system neoplasms. *Diagn Pathol* **11**, 55.

42 Wu G, Diaz AK, Paugh BS, Rankin SL, Ju B, Li Y, Zhu X, Qu C, Chen X, Zhang J *et al.* (2014) The genomic landscape of diffuse intrinsic pontine glioma and pediatric non-brainstem high-grade glioma. *Nat Genet* **46**, 444–450.

43 Tanaka Y, Abe Y, Tsugu A, Takamiya Y, Akatsuka A, Tsuruo T, Yamazaki H, Ueyama Y, Sato O, Tamaoki N *et al.* (1994) Ultrastructural localization of P-glycoprotein on capillary endothelial cells in human gliomas. *Virchows Arch* **425**, 133–138.

44 Richtig E, Asslaber M, Partl R, Avian A, Berghold A, Kapp K, Preusser M, Becker JC and Curiel-Lewandrowski C (2016) Lack of P-glycoprotein expression in melanoma brain metastases of different melanoma types. *Clin Neuropathol* **35**, 89–92.

45 Yonemori K, Tsuta K, Ono M, Shimizu C, Hirakawa A, Hasegawa T, Hatanaka Y, Narita Y, Shibui S and Fujiwara Y (2010) Disruption of the blood brain barrier by brain metastases of triple-negative and basal-type breast cancer but not HER2/neu-positive breast cancer. *Cancer* **116**, 302–308.

46 Uchida Y, Ohtsuki S, Katsukura Y, Ikeda C, Suzuki T, Kamiie J and Terasaki T (2011) Quantitative targeted absolute proteomics of human blood-brain barrier transporters and receptors. *J Neurochem* **117**, 333–345.

47 King AJ, Arnone MR, Bleam MR, Moss KG, Yang J, Fedorowicz KE, Smitheman KN, Erhardt JA, Hughes-Earle A, Kane-Carson LS *et al.* (2013) Dabrafenib; preclinical characterization, increased efficacy when combined with trametinib, while BRAF/MEK tool combination reduced skin lesions. *PLoS One* **8**, e67583.

48 Stuart DD, Li N, Poon DJ, Aardalen K, Kaufman S, Merritt H, Salangsang F, Lorenzana E, Li A, Ghoddusi M *et al.* (2012) Abstract 3790: preclinical profile of LGX818: a potent and selective RAF kinase inhibitor. *Cancer Res* **72**, 3790.

49 Tsai J, Lee JT, Wang W, Zhang J, Cho H, Mamo S, Bremer R, Gillette S, Kong J, Haass NK *et al.* (2008) Discovery of a selective inhibitor of oncogenic B-Raf kinase with potent antimelanoma activity. *Proc Natl Acad Sci USA* **105**, 3041–3046.

50 Falchook GS, Long GV, Kurzrock R, Kim KB, Arkenau HT, Brown MP, Hamid O, Infante JR, Millward M, Pavlick A *et al.* (2014) Dose selection, pharmacokinetics, and pharmacodynamics of BRAF inhibitor dabrafenib (GSK2118436). *Clin Cancer Res* **20**, 4449–4458.

51 Fennira F, Pages C, Schneider P, Sidina I, Viguier M, Basset-Seguin N, Madjlessi-Ezra N, Madelaine I, Bagot M, Battistella M *et al.* (2014) Vemurafenib in the French temporary authorization for use metastatic melanoma cohort: a single-centre trial. *Melanoma Res* **24**, 75–82.

52 Yadav V, Burke TF, Huber L, Van Horn RD, Zhang Y, Buchanan SG, Chan EM, Starling JJ, Beckmann RP and Peng SB (2014) The CDK4/6 inhibitor LY2835219 overcomes vemurafenib resistance resulting from MAPK reactivation and cyclin D1 upregulation. *Mol Cancer Ther* **13**, 2253–2263.

53 Rizos H, Menzies AM, Pupo GM, Carlino MS, Fung C, Hyman J, Haydu LE, Mijatov B, Becker TM, Boyd SC *et al.* (2014) BRAF inhibitor resistance mechanisms in metastatic melanoma: spectrum and clinical impact. *Clin Cancer Res* **20**, 1965–1977.

54 Wang J, Yao Z, Jonsson P, Allen AN, Qin ACR, Uddin S, Dunkel IJ, Petriccione M, Manova K, Haque S *et al.* (2018) A secondary mutation in BRAF confers resistance to RAF inhibition in a BRAF(V600E)-mutant brain tumor. *Cancer Discov* **8**, 1130–1141.

55 Niessner H, Forschner A, Klumpp B, Honegger JB, Witte M, Bornemann A, Dummer R, Adam A, Bauer J, Tabatabai G *et al.* (2013) Targeting hyperactivation of the AKT survival pathway to overcome therapy resistance of melanoma brain metastases. *Cancer Med* **2**, 76–85.

Supporting information

Additional supporting information may be found online in the Supporting Information section at the end of the article.

Fig. S1. Body weight curves from intervention studies presented in Fig. 2. (A) Average mouse body weights from the experiment presented in Fig. 2A-B. Treatment periods are shaded in gray. Data are represented as mean $\pm$ SD (n $\geq$ 7). (B) Average mouse body weights from the experiment presented in Fig. 2D. Treatment period is shaded in gray. Data are represented as mean $\pm$ SD (n $\geq$ 7). (C) Average mouse body weights from the experiment presented in Fig. 2E-F. Treatment period is shaded in gray. Data are represented as mean $\pm$ SD (n $\geq$ 8).